Inorganic Chemistry

Article

pubs.acs.org/IC

Synthesis and Temperature-Induced Structural Phase and Spin Transitions in Hexadecylboron-Capped Cobalt(II) Hexachloroclathrochelate and Its Diamagnetic Iron(II)-Encapsulating Analogue

Anna V. Vologzhanina,*[,†] Alexander S. Belov,[†] Valentin V. Novikov,[†] Alexander V. Dolganov,[†] Galina V. Romanenko,[‡] Victor I. Ovcharenko,[‡] Alexander A. Korlyukov,[†,§] Mikhail I. Buzin,[†] and Yan Z. Voloshin*[,†]

[†]Nesmeyanov Institute of Organoelement Compounds, Russian Academy of Sciences, 119991 Moscow, Russia

[‡]International Tomography Center, Siberian Branch of the Russian Academy of Sciences, 630090 Novosibirsk, Russia

[§]Pirogov Russian National Research Medical University, 117997 Moscow, Russia

Supporting Information

ABSTRACT: Template condensation of dichloroglyoxime with *n*-hexadecylboronic acid on the corresponding metal ion as a matrix under vigorous reaction conditions afforded *n*-hexadecylboron-capped iron and cobalt(II) hexachloroclathrochelates. The complexes obtained were characterized using elemental analysis, MALDI-TOF mass spectrometry, IR, UV−vis, ^{1}H and ^{13}C{^{1}H} NMR, ^{57}Fe Mössbauer spectroscopies, SQUID magnetometry, electron paramagnetic resonance, and cyclic voltammetry (CV) and by X-ray crystallography. The multitemperature single-crystal X-ray diffraction, SQUID magnetometry, and differential scanning calorimetry experiments were performed to study the temperature-induced spin-crossover [for the paramagnetic cobalt(II) complex] and the crystal-to-crystal phase transitions (for both of these clathrochelates) in the solid state. Analysis of their crystal packing using the molecular Voronoi polyhedra and the Hirshfeld surfaces reveals the structural rearrangements of the apical long-chain alkyl substituents resulting from such phase transitions being more pronounced for a macrobicyclic cobalt(II) complex. Its fine-crystalline sample undergoes the gradual and fully reversible spin transition centered at approximately 225 K. The density functional theory calculated parameters for an isolated molecule of this cobalt(II) hexachloroclathrochelate in its low- and high-spin states were found to be in excellent agreement with the experimental data and allowed to localize the spin density within a macrobicyclic framework. CV of the cobalt(II) complex in the cathodic range contains one reversible wave assigned to the $Co^{2+/+}$ redox couple with the reduced anionic cobalt(I)-containing species stabilized by the electronic effect of six strong electron-withdrawing chlorine substituents. The quasireversible character of the $Fe^{2+/+}$ wave suggests that the anionic iron(I)-containing macrobicyclic species undergo substantial structural changes and side chemical reactions after such metal-centered reduction.

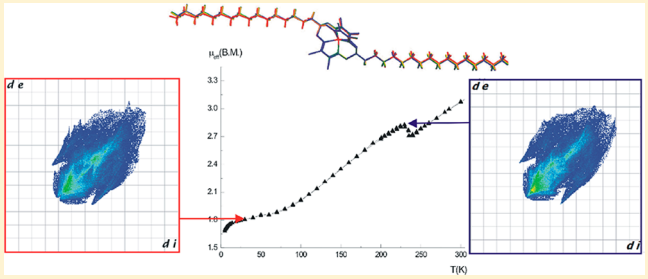

1. INTRODUCTION

A spin-transition phenomenon has raised increasing interest because of its possible practical applications. Spin-crossover (SCO) materials[1] based on molecules that exhibit crossover between the low-spin (LS) and high-spin (HS) states have a potential for data storage[2] and visualization[3] and for molecular electronics as well.[4,5] The family of iron and cobalt(II) cage complexes with apical long-chain alkyl substituents has been previously reported[6−9] as being promising candidate for such materials: even small variations in the chemical nature of the cobalt(II) complexes can significantly modify their SCO characteristics. The acyclic and alicyclic hexadecylboron-capped iron and cobalt(II) macrobicyclic compounds have undergone up to three phase transitions in the temperature range 200−400 K.[10,11] At the same time, all of these aliphatic macrobicyclic metal(II) tris(dioximates) were the LS complexes from 4 to 400 K with $s = 0$ and $^{1}/_{2}$ for the iron and cobalt(II) clathrochelates, respectively. Recently,[12] we discovered a large axial anisotropy of the magnetic susceptibility of the boron-capped cobalt(II) hexachloroclathrochelates in their HS state, reaching as high as 12.6×10^{-32} m^3. This behavior, assigned to a very large zero-field-splitting energy of the caged cobalt(II) ion in a trigonal prismatic N_6-coordination environment, is restricted to its HS state only. The magnetometry data, however, suggested the preferable population of the LS state of this clathrochelate in the solid state at low temperatures. Given that only substitution of the clathrochelate ligand by six halogen

Received: March 10, 2015
Published: May 27, 2015

DOI: 10.1021/acs.inorgchem.5b00546
Inorg. Chem. 2015, 54, 5827−5838

atoms[13−15] resulted in a sufficiently weak ligand field to make HS ↔ LS transitions possible, here we report the synthesis, single-crystal X-ray structures, SCO and phase transition behavior, and magnetic, spectral, and redox properties of the hexadecylboron-capped cobalt(II) hexachloroclathrochelate compared with its iron(II)-containing analogue; note that such metal hexahalogenoclathrochelates are also reported[15,16] to be very efficient electrocatalysts for hydrogen production.

2. EXPERIMENTAL SECTION

Materials and Methods. The reagents used, $CoCl_2·6H_2O$, $FeCl_2·4H_2O$, sorbents, organic bases, and solvents, were obtained commercially (SAF). Hexadecylboronic acid, solvatocomplex $Fe(CH_3CN)_4Cl_2$, and dichloroglyoxime were prepared as described in refs 11, 17, and 18.

Analytical data (carbon, hydrogen, and nitrogen contents) were obtained with a Carlo Erba model 1106 microanalyzer. Iron and cobalt contents were determined spectrophotometrically and by X-ray fluorescence analysis, respectively.

Matrix-assisted laser desorption ionization time-of-flight mass spectrometry (MALDI-TOF-MS) spectra were recorded using a MALDI-TOF-MS Bruker Autoflex II (Bruker Daltonics) mass spectrometer in reflecto-mol mode. The ionization was induced by a UV laser with a wavelength of 337 nm. The samples were applied to a nickel plate, and 2,5-dihydroxybenzoic acid was used as the matrix. The accuracy of the measurements was 0.1%.

IR spectra of the solid samples (KBr tablets) in the range 400−4000 cm^{-1} were recorded with a PerkinElmer FT-IR Spectrum BX II spectrometer; the characteristic bands of the corresponding clathrochelate frameworks are provided in the Experimental Section.

UV−vis spectra of solutions in dichloromethane were recorded in the range 230−900 nm with a Lambda 9 PerkinElmer spectrophotometer. The individual Gaussian components of these spectra were calculated using the *SPECTRA* program.

^1H and ^{13}C NMR spectra were recorded from CD_2Cl_2 solutions with a Bruker Avance 600 spectrometer. The measurements were done using the residual signals of deuterated solvents (CD_2Cl_2: ^1H, 5.32 ppm; ^{13}C, 53.8 ppm) as a reference.

The ^{57}Fe Mössbauer absorption spectrum of the iron complex was recorded at 298 K using a NP-255 spectrometer (Hungary) with a constant-acceleration mode and a symmetrical triangular change in the velocity of a γ-quantum source (^{57}Co in a rhodium matrix with an activity equal to 5 mCu and with a line emission width equal to 0.11 mm s^{-1}). The spectrum was collected with a 511 multichannel analyzer. The speed scale of the spectrometer was calibrated using the spectrum of sodium nitroprusside as a standard. The isomeric shift (IS) values were obtained relative to the center of this spectrum.

The calorimetric studies in the temperature range 150−420 K under argon were performed on a Mettler-822e differential scanning calorimeter; the heating and cooling rates were 10 K min^{-1}.

Cyclic voltammetry (CV) experiments were carried out in dichloromethane solutions with 0.1 M $[(n\text{-}C_4H_9)_4N](BF_4)$ as the supporting electrolyte using a model Parstat 2273 potentiostat (Princeton Applied Research, Oak Ridge, TN) with a conventional and one-compartment three-electrode cell (10 mL of solution). A platinum disk electrode with an active surface area of 0.125 cm^2 was used as the working electrode. The electrode was thoroughly polished and rinsed before measurements. A platinum counter electrode and standard Ag/AgCl/KCl(aq) reference electrode were used. All solutions were thoroughly deaerated by passing argon through the solution before the CV experiments and above the solution during the measurements.

X-band electron paramagnetic resonance (EPR) spectra for the cobalt(II) complex were acquired on a Bruker ElexSys E500 spectrometer, equipped with a ER049X microwave bridge, a SHQ cavity, an Oxford ESR-900 liquid-helium cryostat, and an Oxford ITC 5035 temperature variable unit. The glassy sample for EPR experiments was obtained from a 5 mM toluene solution of this clathrochelate. EPR spectra were registered at the following parameters: microwave frequency 9.38 GHz, microwave power 20.20 mW, modulation frequency 100 kHz, modulation amplitude 8 G, conversion time 81.92 ms, time constant 20.48 ms, and resolution 4096 points. The EPR spectral simulation was performed using *EasySpin*.[19]

The magnetic susceptibility of its polycrystalline samples was measured with a Quantum Design MPMS*XL* SQUID magnetometer in the temperature range 2−300 K with a magnetic field of up to 5 kOe. None of complexes exhibited any field dependence of molar magnetization at low temperatures. The diamagnetic corrections were made using the Pascal constants.[20] The effective magnetic moment was calculated as $\mu_{eff}(T) = [(3k/N_A\mu_B^2)\chi T]^{1/2} \approx (8\chi T)^{1/2}$.

Synthesis. *$Fe(Cl_2Gm)_3(Bn\text{-}C_{16}H_{33})_2$.* Dichloroglyoxime (0.87 g, 5.56 mmol), *n*-hexadecylboronic acid (1.0 g, 3.7 mmol), and solvatocomplex $Fe(CH_3CN)_4Cl_2$ (0.54 g, 1.85 mmol) were dissolved/suspended in dry nitromethane (50 mL) under argon, and then the solvent (10 mL) was partially distilled off from the stirred reaction mixture. The reaction mixture was cooled to room temperature, and the orange-red precipitate was filtered off. The precipitate was washed with 4 M aqueous hydrochloric acid, water, ethanol, diethyl ether, and hexane. Then the product was dissolved in a 1:1 dichloromethane−hexane mixture and flash-chromatographically separated on silica gel (0.035−0.070 mm, 30-mm layer). The filtrate was evaporated to a small volume and precipitated with hexane. The precipitate was filtered off, washed with hexane, and dried in vacuo. Yield: 1.19 g (65%). Anal. Calcd for $C_{38}H_{66}N_6FeO_6Cl_6B_2$: C, 45.92 ; H, 6.65; N, 8.46; Fe, 5.64. Found: C, 46.09; H, 6.74; N, 8.41; Fe, 5.72. MALDI-TOF-MS: *m*/*z* 993 ($[M]^{•+}$). ^1H NMR (CD_2Cl_2): δ 0.52 (m, 4H, CH_2B), 0.77 (m, 6H, CH_3), 1.15−1.26 (m, 56H, $(CH_2)_{14}$). $^{13}C\{^1H\}$ NMR (CD_2Cl_2): δ 15.87 (s, CH_3), 18.30 (s, CH_2B), 24.71 (s, 15-CH_2), 25.63 (s, 2-CH_2), 31.38−31.79 (ms, $(CH_2)_9CH_3$), 33.97 (s, 14-CH_2), 34.69 (s, 3-CH_2), 132.58 (s, C═N). IR (cm^{-1}, KBr): ν(C═N) 1528; ν(N−O) 842, 884, 901, 947; ν(B−O) 1099m. UV−vis [CH_2Cl_2; λ_{max}, nm ($\varepsilon \times 10^{-3}$, mol^{-1} L cm^{-1})]: 264 (9.6), 286 (3.2), 297 (3.5), 383 (2.9), 422 (7.0), 454 (12), 491 (3.3). ^{57}Fe Mössbauer spectrum (mm s^{-1}): IS = 0.39; QS = 1.21.

$Co(Cl_2Gm)_3(Bn\text{-}C_{16}H_{33})_2$. Dichloroglyoxime (0.44 g, 2.78 mmol), *n*-hexadecylboronic acid (0.50 g, 1.85 mmol), and $CoCl_2$ (0.12 g, 0.93 mmol) were dissolved/suspended in dry nitromethane (20 mL) under argon, and then the solvent (10 mL) was partially distilled off. The reaction mixture was cooled to room temperature, and the dark-brown precipitate was filtered off and washed with 4 M aqueous hydrochloric acid, water, ethanol, diethyl ether, and hexane. The product was recrystallized from hot chlorobenzene and then extracted with chlorobenzene, and the extract was flash-chromatographically separated on silica gel (0.035−0.070 mm, 30-mm layer). The filtrate was evaporated to a small volume and precipitated with hexane. The precipitate was washed with hexane and dried in vacuo. Yield: 0.55 g (60%). Anal. Calcd for $C_{38}H_{66}N_6CoO_6Cl_6B_2$: C, 45.78; H, 6.63; N, 8.43; Co, 5.92. Found: C, 45.91; H, 6.61; N, 8.36; Co, 5.80. MALDI-TOF-MS: *m*/*z* 996 ($[M]^{•+}$). ^1H NMR (CD_2Cl_2): δ 0.76 (m, 6H, CH_3), 1.31 (m, 8H, 14,15-CH_2), 1.45 (m, 4H, 13-CH_2), 1.59 (m, 4H, 12-CH_2), 1.80 (m, 4H, 11-CH_2), 2.10 (m, 4H, 10-CH_2), 2.53 (m, 4H, 9-CH_2), 3.18 (m, 4H, 8-CH_2), 4.12 (m, 4H, 7-CH_2), 5.52 (m, 4H, 6-CH_2), 7.59 (m, 4H, 5-CH_2), 11.04 (s, 4H, 4-CH_2), 16.69 (s, 4H, 3-CH_2), 29.17 (s, 4H, 2-CH_2), 39.41 (s, 4H, CH_2B). $^{13}C\{^1H\}$ NMR (CD_2Cl_2): δ 15.84 (s, CH_3), 24.80 (s, 15-CH_2), 31.70 (s, 13-CH_2), 32.09 (s, 12-CH_2), 32.36 (s, 11-CH_2), 32.68 (s, 10-CH_2), 33.14 (s, 9-CH_2), 34.10 (s, 14-CH_2), 34.81 (s, 8-CH_2), 36.34 (s, 7-CH_2), 38.63 (s, 6-CH_2), 42.33 (s, 5-CH_2), 53.73 (s, 4-CH_2). IR (cm^{-1}, KBr): ν(C═N) 1556; ν(N−O) 870, 902, 941, 976; ν(B−O) 1096m. UV−vis [CH_2Cl_2; λ_{max}, nm ($\varepsilon \times 10^{-3}$, mol^{-1} L cm^{-1})]: 255 (14), 269 (16), 285 (3.0), 296 (5.4), 333 (3.5), 367 (2.9), 436 (1.7), 471 (1.9).

Single-Crystal X-ray Analysis. Single crystals of the complexes $Co(Cl_2Gm)_3(Bn\text{-}C_{16}H_{33})_2$ and $Fe(Cl_2Gm)_3(Bn\text{-}C_{16}H_{33})_2$ were grown from their saturated solutions in a dichloromethane−hexane mixture at room temperature. The intensities of the reflections were measured with a Bruker Apex II CCD diffractometer using graphite-monochromated Mo Kα radiation (λ = 0.71073 Å). The structures were solved by direct methods and refined by full-matrix least squares

DOI: 10.1021/acs.inorgchem.5b00546
Inorg. Chem. 2015, 54, 5827−5838

Table 1. Crystallographic Data, Refinement Parameters, and Some Geometrical Parameters for the First X-rayed Single Crystal of the Clathrochelate $Co(Cl_2Gm)_3(Bn\text{-}C_{16}H_{33})_2$ at Different Temperatures

	temperature (K)				
	295	260	240	230	40
space group			*C*2/*c*		
Z			4		
a (Å)	45.321(3)	45.150(9)	45.092(8)	45.071(6)	43.99(2)
b (Å)	7.9660(10)	7.929(2)	7.9210(13)	7.9023(13)	7.938(4)
c (Å)	14.0030(10)	13.960(3)	13.924(2)	13.9272(16)	13.853(8)
β (deg)	101.675(5)	101.97(3)	102.02(2)	102.261(16)	101.225(11)
V (Å^3)	4950.9(8)	4888.8(18)	4864.0(14)	4847.2(11)	4745(4)
d_{calc} (mg m^{-3})	1.337	1.354	1.360	1.365	1.394
μ (mm^{-1})	0.718	0.727	0.730	0.733	0.749
measd/indep/obsd I_{hkl}	14276/4830/1908	14056/4764/2144	22458/4750/2283	13499/4602/2128	13674/4596/2329
R_{int}	0.0925	0.0913	0.1321	0.1035	0.1611
data/param/restraints	4830/260/4	4764/268/0	4750/268/0	4602/268/0	4596/268/12
R1/wR2/GOF	0.044/0.086/0.894	0.040/0.077/0.874	0.047/0.091/1.009	0.047/0.081/0.839	0.077/0.1759/1.024
Co−N(1) (Å)	2.015(3)	1.998(3)	1.991(3)	1.989(3)	1.908(5)
Co−N(2) (Å)	1.970(3)	1.960(2)	1.969(3)	1.975(3)	2.012(5)
Co−N(3) (Å)	1.995(3)	1.988(3)	1.978(3)	1.958(3)	2.031(5)
	av. 1.993	av. 1.982	av. 1.979	av. 1.974	av. 1.984
φ (deg)	1.9	2.1	2.3	2.2	3.1
α (deg)	39.1	38.8	39.1	38.9	39.2
h (Å)	2.51	2.49	2.49	2.48	2.51

Table 2. Crystallographic Data, Refinement Parameters and Some Geometrical Parameters for the Second X-rayed Single Crystal of the Clathrochelate $Co(Cl_2Gm)_3(Bn\text{-}C_{16}H_{33})_2$ at Different Temperatures

	temperature (K)					
	cooling			heating		
	270	251	225	235	261	283
space group			*C*2/*c*			
Z			4			
a (Å)	45.282(4)	45.225(3)	44.373(3)	45.1402(15)	45.270(6)	45.426(18)
b (Å)	7.9411(8)	7.9329(5)	7.9331(5)	7.9183(3)	7.9381(11)	7.976(3)
c (Å)	13.9696(13)	13.9555(9)	13.9724(9)	13.9377(5)	13.9642(19)	14.016(6)
β (deg)	101.799(7)	101.983(4)	100.627(7)	102.137(2)	101.918(9)	101.775(9)
V (Å^3)	4917.2(8)	4897.6(5)	4834.1(5)	4870.4(3)	4910.0(12)	4972(3)
d_{calc} (mg m^{-3})	1.346	1.351	1.369	1.359	1.348	1.331
μ (mm^{-1})	0.723	0.725	0.735	0.729	0.724	0.715
measd/indep/obsd I_{hkl}	18898/4831/2290	19987/4803/2196	34811/4731/2720	19620/4772/2646	18371/4804/2067	19332/4882/1772
R_{int}	0.1428	0.1579	0.1654	0.1498	0.1678	0.1361
data/param/restraints	4831/268/0	4803/268/0	1731/268/0	4772/268/0	4804/268/0	4882/268/0
R1/wR2/GOF	0.054/0.099/0.939	0.057/0.152/1.006	0.065/0.169/1.003	0.054/0.096/0.980	0.057/0.100/0.838	0.048/0.099/0.857
Co−N(1) (Å)	2.010(3)	1.993(3)	2.006(4)	1.991(2)	2.003(3)	2.004(3)
Co−N(2) (Å)	1.971(3)	1.964(3)	1.970(4)	1.963(2)	1.973(3)	1.985(3)
Co−N(3) (Å)	1.982(3)	1.979(3)	1.981(3)	1.982(2)	1.997(3)	1.979(3)
	av. 1.988	av. 1.979	av. 1.986	av. 1.979	av. 1.991	av. 1.989
φ (deg)	2.1	2.2	1.6	2.4	2.1	2.2
α (deg)	38.9	39.0	39.0	38.9	39.0	38.9
h (Å)	2.50	2.49	2.50	2.48	2.51	2.50

against F^2. Non-hydrogen atoms were refined in an anisotropic approximation except that for the disordered fragments. The molecule $Co(Cl_2Gm)_3(Bn\text{-}C_{16}H_{33})$ was found to be disordered at room temperature: C17, C18, and C19 carbon atoms of its hexadecyl apical substituent were equally disordered over two sites, and they were refined isotropically with C17−C18 and C18−C19 distances fixed at 1.5 Å. The positions of the hydrogen atoms were calculated, and the H(C) atoms were included in the refinement by the riding model with $U_{iso}(H) = nU_{eq}(C)$, where n = 1.5 for methyl groups and 1.2 for the other atoms. All calculations were made using the *SHELXS.0*[21] and *OLEX2*[22] program packages.

As follows from differential scanning calorimetry (DSC) data (vide infra), both of these cage complexes undergo temperature-phase transitions. So, multitemperature X-ray diffraction (XRD) studies of one single crystal of the iron(II) cage complex and two single crystals of cobalt(II) clathrochelate were performed; the details of data collection and refinement parameters are listed in Tables 1−3. Specific features of the intermolecular interactions in the crystals $Co(Cl_2Gm)_3(Bn\text{-}C_{16}H_{33})_2$ and $Fe(Cl_2Gm)_3(Bn\text{-}C_{16}H_{33})_2$ were studied on the basis of molecular Voronoi[23,24] and Hirshfeld surface[25,26] approaches using the program packages *ToposPro*[27] and *CrystalExplorer3.0*,[28] respectively.

DOI: 10.1021/acs.inorgchem.5b00546
Inorg. Chem. 2015, 54, 5827−5838

Table 3. Crystallographic Data, Refinement Parameters and Some Geometrical Parameters for the Complex $Fe(Cl_2Gm)_3(Bn\text{-}C_{16}H_{33})_2$ at Different Temperatures

	temperature (K)				
	168	173	178	183	240
space group			C2/c		
Z			4		
a (Å)	44.739(4)	44.7655(19)	44.755(2)	44.763(8)	44.925(4)
b (Å)	7.8988(8)	7.9046(4)	7.9093(4)	7.9062(14)	7.9417(6)
c (Å)	13.8864(14)	13.8872(6)	13.9055(7)	13.905(3)	13.9468(11)
β (deg)	102.504(4)	102.430(3)	102.436(3)	102.387(4)	102.069(6)
V (Å^3)	4790.9(8)	4798.8(4)	4808.3(17)	4806.6(15)	4865.7(7)
d_{calc} (mg m^{-3})	1.377	1.375	1.372	1.372	1.356
μ (mm^{-1})	0.698	0.697	0.696	0.696	0.687
measd/indep/obsd I_{hkl}	17047/4706/2614	18541/4713/2696	18696/4703/2610	18489/4715/2623	17359/4763/2277
R_{int}	0.1101	0.0989	0.0935	0.1077	0.1223
data/param/restraints	4706/268/0	4713/268/0	4703/268/0	4715/268/0	4763/268/0
R1/wR2/GOF	0.047/0.082/0.951	0.047/0.072/0.972	0.045/0.072/0.973	0.042/0.075/0.873	0.044/0.082/0.827
Fe–N(1) (Å)	1.918(3)	1.915(2)	1.916(2)	1.909(2)	1.914(3)
Fe–N(2) (Å)	1.916(3)	1.906(2)	1.911(2)	1.911(2)	1.904(3)
Fe–N(3) (Å)	1.922(3)	1.923(2)	1.926(2)	1.922(2)	1.921(3)
	av. 1.919	av. 1.915	av. 1.918	av. 1.914	av. 1.913
φ (deg)	18.7	18.9	18.6	18.3	17.5
α (deg)	39.6	39.6	39.6	39.5	39.3
h (Å)	2.40	2.39	2.40	2.39	2.38

Scheme 1. Synthesis of the Hexadecylboron-Capped Iron and Cobalt(II) Hexachloroclathrochelates

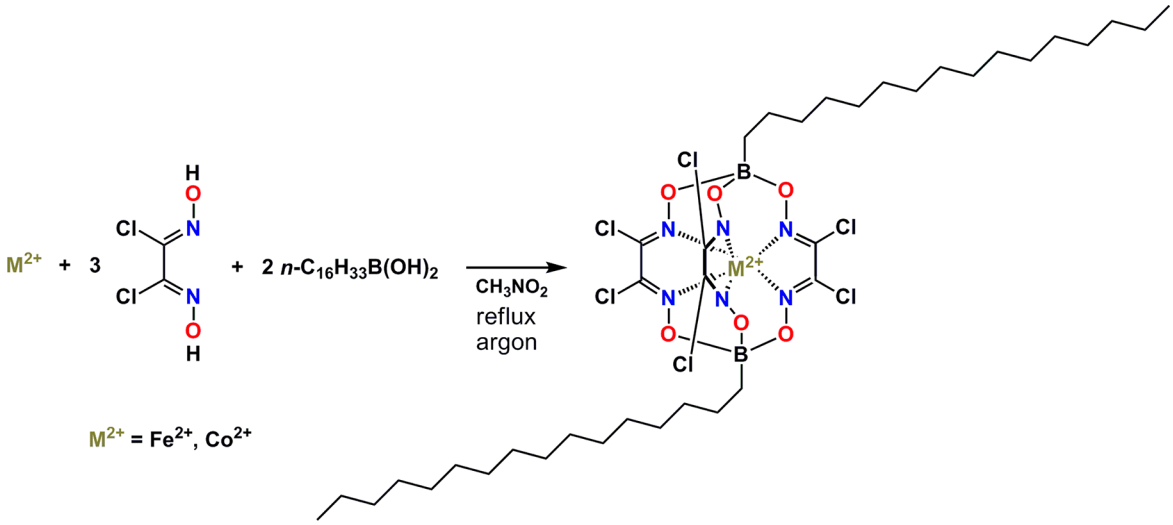

Computational Details. The quantum-chemical calculations using the *Gaussian 09* program suite[29] were performed to study the charge and spin distributions in the isolated molecule $Co(Cl_2Gm)_3(Bn\text{-}C_{16}H_{33})$. The B3LYP hybrid functional and 6-311G(d,p) basis set were utilized for geometry optimization and spin-density calculations of its LS (doublet) and HS (quartet) states. For such geometry optimizations, the single-crystal XRD data for this cobalt(II) complex at 40 and 273 K were used as initial approximations for doublet and quartet states, respectively. The optimization was carried out in the C_2 point group for its macrobicyclic molecule, and the optimized structures of such LS and HS states, characterized using Hessian matrix calculations, revealed the absence of positive eigenvalues. The spin densities were calculated as the difference between the densities of α and β electrons; their isosurfaces were drawn using the *ChemCraft* program.[30]

3. RESULTS AND DISCUSSION

Synthesis. Hexadecylboron-capped iron and cobalt(II) hexachloroclathrochelates were obtained by Scheme 1 using direct template condensation of three dichloroglyoxime molecules with Lewis acidic *n*-hexadecylboronic acid as the cross-linking agent on the Fe^{2+} and Co^{2+} ions as matrices. Such macrobicyclic complexes were isolated in moderate yields under vigorous reaction conditions (a reflux in high-boiling polar aprotic nitromethane as the reaction medium followed by a further partial azeotropic distillation of the solvent) because of the poor donor ability of dichloroglyoxime; we failed to obtain these cage complexes in other aprotic solvents (in particular, acetonitrile). Water and HCl released from this template condensation were azeotropically distilled off with nitromethane, shifting an equilibrium in the direction of a target clathrochelate. However, given the high volatility of *n*-

DOI: 10.1021/acs.inorgchem.5b00546
Inorg. Chem. 2015, 54, 5827–5838

Table 4. Oxidation (E^{ox}) and Reduction (E^{red}) Potentials (mV) and the Characteristics of These Electrochemical Processes for the Hexadecylboron-Capped Iron and Cobalt(II) Hexachloroclathrochelates

	oxidation				reduction			
complex	E_p^a	E_p^c	ΔE	I_c/I_a	E_p^c	E_p^a	ΔE	I_c/I_a
$Fe(Cl_2Gm)_3(Bn\text{-}C_{16}H_{33})_2$	1920	1790	130	0.55	−500	−360	140	0.87
$Co(Cl_2Gm)_3(Bn\text{-}C_{16}H_{33})_2$	1170	1060	110	0.85	10	70	60	1

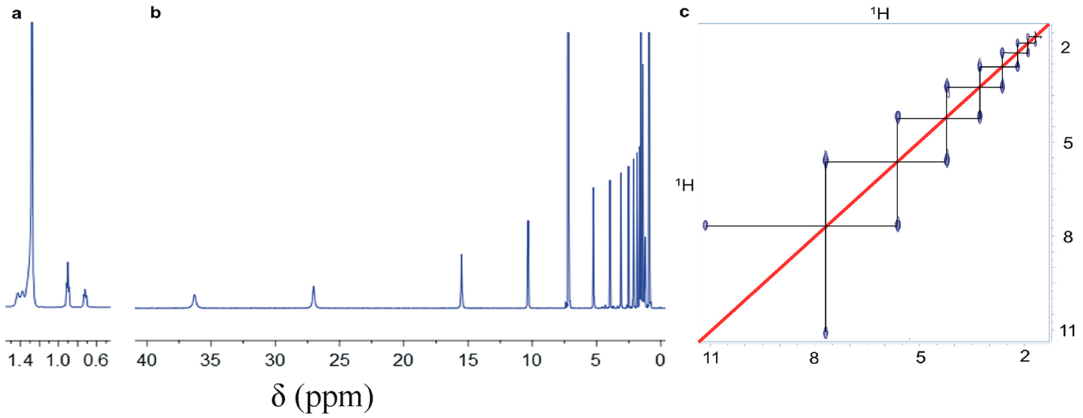

Figure 1. ^1H NMR spectra (600 MHz, $CDCl_3$, 298 K) of the diamagnetic complex $Fe(Cl_2Gm)_3(Bn\text{-}C_{16}H_{33})_2$ (a), the paramagnetic clathrochelate $Co(Cl_2Gm)_3(Bn\text{-}C_{16}H_{33})_2$ (b), and the part of its 2D $^1H-^1H$ COSY spectrum (c) showing an increase in the paramagnetic shift along the hexadecyl aliphatic chain (the diagonal was suppressed using a convolution processing procedure to enhance the resolution in an upfield region).

hexadecylboronic acid (t_{subl} is approximately 91−94 °C), it also has been partially distilled off from the reaction mixture, and this is the reason why the reaction mixture was efficiently refluxed at the first stage of this synthetic procedure; the side processes of protolytic cleavage of the B−C bond were observed in the reaction mixture.

Spectral Studies. IR spectra of the complexes obtained contain the C═N, N−O, and B−O bond stretching vibrations characteristic of the boron-capped tris(dioximate) clathrochelates. The essential (up to 50 cm^{-1}) differences were observed between ν(C═N) for cobalt(II) hexachloroclathrochelate and those of its aliphatic and especially aromatic macrobicyclic analogues. Such a ν(C═N) band in this spectrum is substantially (by approximately 30 cm^{-1}) shifted in the high-frequency region compared with that for its iron(II)-encapsulating analogue.

The solution UV−vis spectrum of the clathrochelate $Fe(Cl_2Gm)_3(Bn\text{-}C_{16}H_{33})_2$ contains in the visible range four intensive [$\varepsilon \sim (2-10) \times 10^3$ L mol^{-1} cm^{-1}] Fe d → Lπ* metal-to-ligand charge-transfer (MLCT) bands with maxima from 430 to 490 nm, while that of the complex $Co(Cl_2Gm)_3(Bn\text{-}C_{16}H_{33})_2$ shows only two less intensive [$\varepsilon \sim (1-2) \times 10^3$ mol^{-1} L cm^{-3}] Co d → Lπ* MLCT bands at 437 and 471 nm.

The IS value in the ^{57}Fe Mössbauer spectrum of the clathrochelate $Fe(Cl_2Gm)_3(Bn\text{-}C_{16}H_{33})_2$ is characteristic of the LS iron(II) complexes, whereas the quadrupole splitting (QS) value indicates a substantial trigonal prismatic distortion of its FeN_6-coordination polyhedron. The QS value deduced for this cage complex using the partial QS concept[31,32] from the equation QS = 6−9[$\cos^2 \alpha/\cos^2(\varphi/2)$], is approximately 0.49 mm s^{-1}. The substantial difference between the experimentally obtained and deduced QSs (approximately 0.72 mm s^{-1}) can be explained by the electronic effect of two negatively charged capping tetrahedral O_3BC groups and by the crystal-packing effects. Indeed, the latter effect for all of the to date X-rayed iron(II) hexachloroclathrochelates falls in the range 0.15−0.30 mm s^{-1} [see Table S1 in the Supporting Information (SI)].

Electrochemistry. The redox characteristics of these iron and cobalt hexachloroclathrochelates were studied using CV. The redox waves in their CVs correspond to the diffusion-controlled current processes (as follows from the linear plot of I_p versus $\nu^{1/2}$, where ν is the scan rate); the correspondent potential values and characteristics of the electrochemical processes are collected in Table 4. These CVs in the anodic range contain one-electron waves assigned to the metal-centered $M^{2+/3+}$ oxidations. Six strong electron-withdrawing chlorine atoms in the ribbed chelate fragments of their macrobicyclic ligand substantially decrease the energy of its highest occupied molecular orbital. The differences between the peaks of direct oxidation and backward rereduction reactions ($\Delta E = E^{ox} - E^{red}$) are equal to 110 and 130 mV, respectively, while the current ratios of the direct and reverse peaks, characterizing a reversibility of the redox processes, are equal to 0.85 and 0.55, respectively. This suggests their quasireversibility, and the substantial structural changes in the cationic metal(III)-containing clathrochelate species resulted from such electrochemical oxidation.

CV of the complex $Co(Cl_2Gm)_3(Bn\text{-}C_{16}H_{33})_2$ in the cathodic range contains one reversible wave with ΔE = 60 mV and with the current ratio equal to 1 assigned to metal-centered $Co^{2+/+}$ reduction. This suggests the absence of any structural changes and side chemical reactions of the reduced anionic cobalt(I)-containing species stabilized by the electronic effect of six strong electron-withdrawning chlorine substituents at its cage framework. At the same time, the analogous $Fe^{2+/+}$ redox process is quasireversible with ΔE = 140 mV, suggesting the substantial structural changes and side chemical reactions of the anionic iron(I)-containing macrobicyclic species.

Magnetic Resonance Spectroscopy. Cobalt(II) hexachloroclathrochelates have been recently shown to undergo unusual anticooperative $^1/_2 \Leftrightarrow {}^3/_2$ spin transition,[33] implying

DOI: 10.1021/acs.inorgchem.5b00546
Inorg. Chem. 2015, 54, 5827−5838

that the population of their HS state is higher in solution than in the solid state. Although the complex $Co(Cl_2Gm)_3(Bn\text{-}C_{16}H_{33})_2$ was reported to be entirely HS in solution at room temperature,[12] lowering the temperature or measuring the magnetic properties in the solid state was expected to lead to the preferential or even full population of its LS state. To probe the magnetic behavior of this cobalt(II) complex in the different conditions, we used NMR (solution, 298 K), EPR (frozen solution, 30 K), and SQUID magnetometry (solid state, 2−340 K).

The ^1H and ^{13}C NMR spectra of the diamagnetic iron(II) complex confirmed its composition, although the apical hexadecyl substituents resulted in a heavily overlapped set of signals in the ^1H NMR spectrum (Figure 1a). The paramagnetic nature of an encapsulated cobalt(II) ion in the complex $Co(Cl_2Gm)_3(Bn\text{-}C_{16}H_{33})_2$ with the same macrobicyclic ligand caused very large downfield paramagnetic shifts of all of the nuclei of its apical hexadecyl substituents, so the corresponding ^1H NMR spectrum contains 16 well-resolved signals (Figure 1b). The paramagnetic shift is pseudocontact in nature and thus depends on the intermolecular distances: the closer the nucleus is to the paramagnetic encapsulated metallocenter, the larger its chemical shift is (Figure 1c).

Recently,[12] we have reported a detailed analysis of the origins of this paramagnetic behavior, which is characteristic of a preferential population of the HS state of such a cobalt(II) complex in solution at room temperature; the paramagnetic shifts for the LS cobalt(II) clathrochelates were shown to have significantly lower magnitude and an opposite sign.[11]

Decreasing the temperature resulted in a steady increase in the paramagnetic shifts according to the Curie law; even at 200 K, no evidence for the population of the LS state was found. Because further lowering of the temperature in the NMR experiment was not possible, we used EPR spectroscopy to study the spin state of $Co(Cl_2Gm)_3(Bn\text{-}C_{16}H_{33})_2$ at low temperature. The X-band EPR spectrum of its frozen toluene solution at 30 K (Figure 2) is characteristic of the LS cobalt(II) clathrochelates;[13] both **g** and hyperfine tensors are rhombic, and the spectrum contains well-resolved eight-line splitting in the downfield region caused by the hyperfine interaction with the ^{59}Co nucleus ($I_{Co} = {}^7/_2$). Additional splitting with the signal ratio 1:2:3:2:1 is observed in the second-derivative spectrum; this pattern was previously assigned[13] to the superhyperfine interaction with two ^{14}N ($I_N = 1$) nuclei of one of the three chelate fragments. Density functional theory (DFT) calculations of the spin-density distribution have confirmed the significant delocalization of an unpaired electron over two nitrogen atoms of the α-dioximate ribbed fragment having the largest Co−N bond lengths (vide supra). This lowering of the molecular symmetry results from Jahn−Teller distortion for the LS electronic configuration d^7, thus confirming the LS nature of the clathrochelate $Co(Cl_2Gm)_3(Bn\text{-}C_{16}H_{33})_2$ at 30 K. The intensity of its EPR spectrum decreases substantially after the temperature is increased, owing to both the loss of spin polarization and the depopulation of the LS state caused by the ${}^1/_2 \Leftrightarrow {}^3/_2$ SCO.[33] The signals of the HS species were not observed at any temperature because the HS cobalt(II) clathrochelates are EPR-silent in the X-band owing to very large negative zero-field-splitting energy and fast transverse relaxation.[12] Thus, the magnetic properties of $Co(Cl_2Gm)_3(Bn\text{-}C_{16}H_{33})_2$ in solution are identical with those of its recently reported analogue $Co(Cl_2Gm)_3(BCH_3)_2$,[33] which implies only a small influence of the nature of apical substituents on a spin state of the cobalt(II) hexachloroclathrochelates.

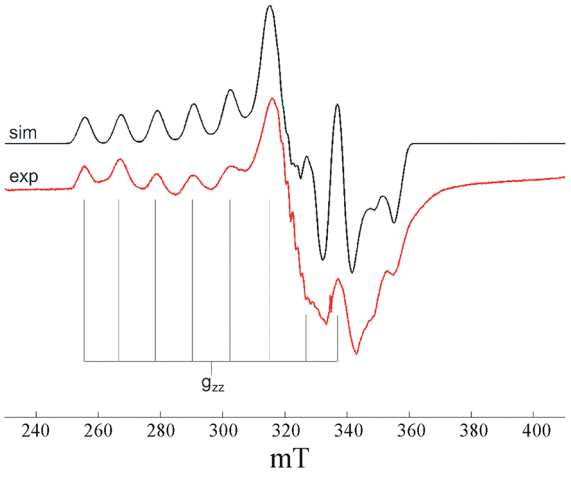

Figure 2. Experimental and simulated X-band EPR spectra of a 5 mM frozen toluene solution of $Co(Cl_2Gm)_3(Bn\text{-}C_{16}H_{33})_2$ at 30 K. The simulated spectra were obtained using the following parameters: g_{xx} = 1.980; g_{yy} = 2.086; g_{zz} = 2.260; A_{xx} = 130 MHz; A_{yy} = 15 MHz; A_{zz} = 370 MHz; $A_{iso}(^{14}N)$ = 42 MHz.

SQUID Magnetometry. In the solid state, however, the apical substituents at a cage framework affect the magnetic properties of such macrobicyclic complexes. Indeed, as follows from the SQUID magnetometry data (Figure 3), the hexadecylboron-capped cobalt(II) clathrochelate is the LS complex below 50 K (μ_{eff} = 1.83 μ_B at 50 K); a gradual increase in its effective magnetic moment is observed at higher temperatures. The SCO is not complete (the μ_{eff} value is significantly lower than the spin-only value of a HS complex) even at 340 K, confirming the anticooperative behavior of the clathrochelate $Co(Cl_2Gm)_3(Bn\text{-}C_{16}H_{33})_2$.

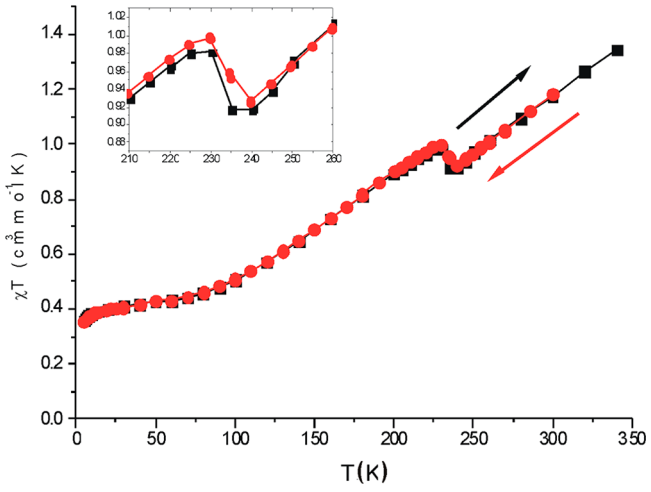

Figure 3. Variable-temperature magnetic susceptibility data for a microcrystalline sample of the clathrochelate $Co(Cl_2Gm)_3(Bn\text{-}C_{16}H_{33})_2$ upon cooling (●) and heating (■) of the sample. Inset: "reverse" fragment of the curve around 230 K.

An unusual feature of these SQUID data is an abrupt drop of the effective magnetic moment at 230 K. Note that this behavior was reproduced repeatedly using different samples and with different experimental setups; the shape of this curve was the same upon heating and cooling of the sample. A similar

DOI: 10.1021/acs.inorgchem.5b00546
Inorg. Chem. 2015, 54, 5827−5838

Table 5. DSC Data on Phase Transitions for the Hexadecylboron-Capped Iron and Cobalt(II) Hexachloroclathrochelates

	crystal-to-crystal phase transitions					
	1 ↔ 2		2 ↔ 3		melting	
complex	T (K)	ΔH (kJ mol^{-1})	T (K)	ΔH (kJ mol^{-1})	T (K)	ΔH (kJ mol^{-1})
$Fe(Cl_2Gm)_3(Bn\text{-}C_{16}H_{33})_2$	173[a]	3.97			408	94.34
$Co(Cl_2Gm)_3(Bn\text{-}C_{16}H_{33})_2$	250	1.35	273	1.21	412	94.60
	250[a]	0.45[a]			412[a]	94.60[b]

[a]Transition temperatures and the heat stored upon a second heating after melting. [b]Second heating after melting.

"reverse" SCO has been previously described for the cobalt(II) complexes, with long-chain alkyl substituents being assigned to a structural phase transition.[9] To gain insight into the nature of the observed magnetic anomaly, we used DSC and XRD experiments.

Crystal-to-Crystal Phase Transitions and DFT Calculations. The fine-crystalline samples of these iron and cobalt(II) hexachloroclathrochelates were studied by DSC in the temperature range 150−420 K; the characteristics of the observed phase transitions are listed in Table 5.

The DSC experiment for iron(II) clathrochelate revealed only one phase transition before melting at T_{C-C} = 173 K, while the curve for its cobalt(II)-encapsulating analogue showed two crystal-to-crystal transitions in this temperature range (Table 5). The heating of the fine-crystalline sample of $Co(Cl_2Gm)_3(Bn\text{-}C_{16}H_{33})_2$ resulted in phase transitions at 250 and 273 K (Figure 4). Note that the temperatures of these

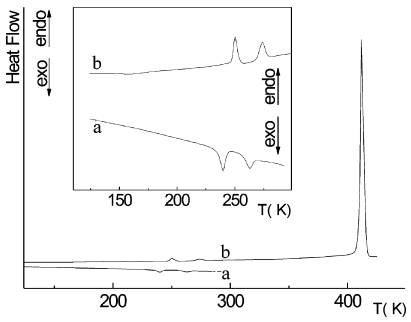

Figure 4. DSC curves for the fine-crystalline sample of the clathrochelate $Co(Cl_2Gm)_3(Bn\text{-}C_{16}H_{33})_2$ upon cooling (a) and heating (b).

crystal-to-crystal transitions exhibit hysteresis and significantly differ from the transition temperature, detected by SQUID magnetometry, even if the same rate of heating/cooling is employed in both of these experiments.

In order to assign a type of crystal-to-crystal phase transition for the clathrochelates $Fe(Cl_2Gm)_3(Bn\text{-}C_{16}H_{33})_2$ and $Co(Cl_2Gm)_3(Bn\text{-}C_{16}H_{33})_2$, we performed a multitemperature single-crystal XRD study. These complexes are isostructural above 40 K (Tables 1 −3). The single-crystal XRD study did not reveal any space group changes, abrupt changes in the cell parameters (Figure S1 in the SI), or substantial distortion of the coordination polyhedron of an encapsulated metal ion (Tables 2 and 3). The molecular structures of these clathrochelates are shown in Figure 5; the main experimental X-rayed geometrical parameters of their molecules at selected temperatures and those theoretically calculated for an isolated molecule, $Co(Cl_2Gm)_3(Bn\text{-}C_{16}H_{33})_2$, in its doublet and quartet states are listed in Table 6 (the main parameters for other temperatures are summarized in Tables 1−3). The rigidity of chelate N═C−C═N fragments caused the remainder of the bite angle α (half of chelate N−M−N angle), whereas the heights h of their MN_6-coordination polyhedra change with a distortion of these macrobicyclic frameworks around the molecular C_3 pseudoaxis (the distortion angle φ is equal to 0° for a trigonal prism, TP, and to 60° for a trigonal antiprism, TAP). TAP geometry is energetically preferable for electronic configurations d^6 and d^7,[34] whereas encapsulation of a metal ion with a high Shannon radius by a rigid pseudoaromatic polyazomethine macrobicyclic ligand and sterical hindrances between the bulky ribbed substituents in α-dioximate chelate fragments of a cage framework cause a TP distortion of such geometry. In this case, such distortion is affected mainly by the nature of an encapsulated metal ion: a FeN_6-coordination polyhedron possesses a geometry intermediate between that of a TP and a TAP (at 240 K, φ = 17.5° and h = 2.38 Å; Table 6), whereas a CoN_6-coordination polyhedron undergoes a translational−rotational expansion because of the higher Shannon radius of the HS Co^{2+} ion (r_i = 0.885 Å) compared with that of the LS Fe^{2+} ion (r_i = 0.75 Å), leading to an increase in the h value at the same temperature up to approximately 2.50 Å in this almost TP coordination polyhedron with φ = 1.9°.

The geometry of a CoN_6-coordination polyhedron in the molecule $Co(Cl_2Gm)_3(Bn\text{-}C_{16}H_{33})_2$ from 40 to 295 K can be considered as a superposition of the doublet and quartet states of this cage complex. Theoretical calculations can be useful to study the LS and HS states of an isolated molecule, $Co(Cl_2Gm)_3(Bn\text{-}C_{16}H_{33})_2$, thus giving us, at least, the qualitative measure of an effect of its crystal packing on the spin-density distribution. In general, the performed quantum-chemical DFT calculation of the LS state of this complex (Table 6) reproduced the distribution of its Co−N bonds at 40 K; however, the calculated Co1−N3 distance (2.156 Å) is substantially different from the experimental one [2.031(5) Å], being greater than the differences for the Co1−N1 and Co−N2 distances (1.910 and 1.970 Å compared with 1.908(5) and 2.012 Å, respectively). This fact, together with the substantial difference between the calculated and experimental φ values (17.6 and 3.1°, respectively) for an isolated cage molecule in its LS state and that in crystal at 40 K, can be explained by the anisotropy of a thermal ellipsoid of a caged Co^{2+} ion affecting the φ and Δ values. In the case of a HS molecule of $Co(Cl_2Gm)_3(Bn\text{-}C_{16}H_{33})_2$, such Co−N distances are also overestimated up to 0.09 Å compared with the experimental values at 295 K (Table 6). Besides, the X-rayed Co−N bond lengths at 295 K are more alternated than those in the calculated isolated HS molecule because of incomplete SCO at this temperature.

To evaluate the character of the spin-density distribution, its isosurfaces were drawn for the LS and HS states of this cobalt(II) clathrochelate (Figure 6). In both of these cases, such density is concentrated within a cage framework localizing close

DOI: 10.1021/acs.inorgchem.5b00546
Inorg. Chem. 2015, 54, 5827−5838

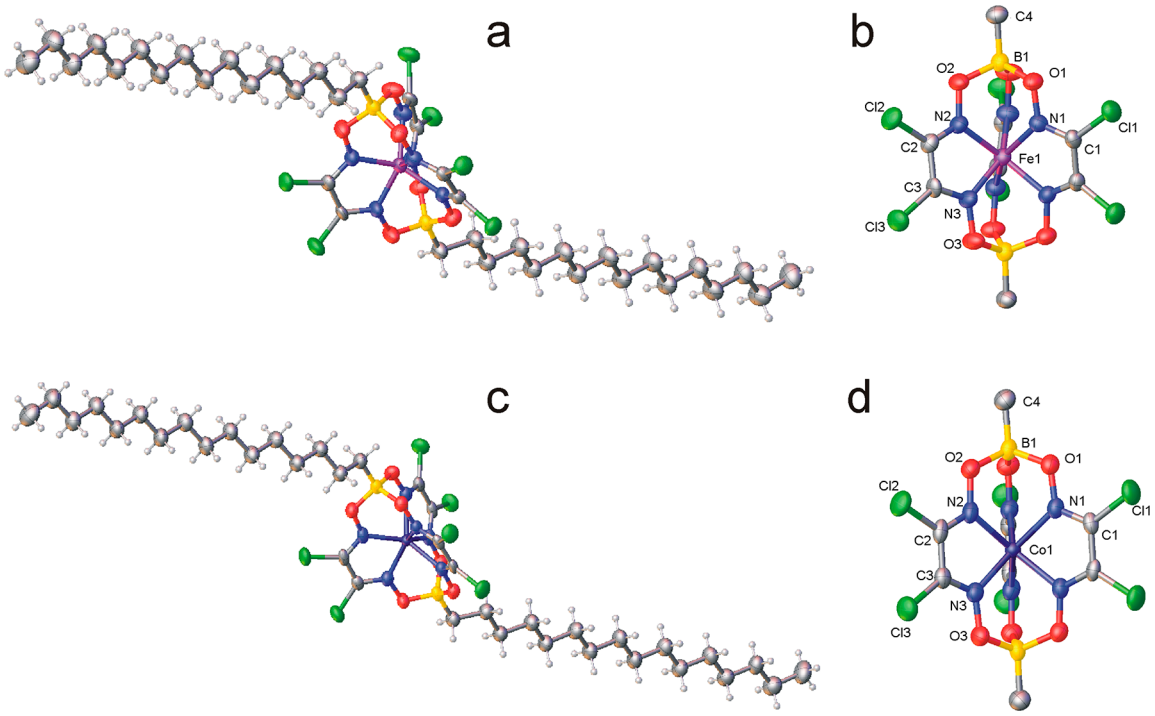

Figure 5. General views of the clathrochelates $Fe(Cl_2Gm)_3(Bn\text{-}C_{16}H_{33})_2$ (a) and $Co(Cl_2Gm)_3(Bn\text{-}C_{16}H_{33})_2$ (c) and their corresponding clathrochelate cages (b and d) given in thermal ellipsoids drawn at the p = 50% level. Only symmetrically independent atoms are labeled.

Table 6. Main X-rayed and DFT-Calculated Geometrical Parameters of the Molecules $Fe(Cl_2Gm)_3(Bn\text{-}C_{16}H_{33})_2$ and $Co(Cl_2Gm)_3(Bn\text{-}C_{16}H_{33})_2$

	$Fe(Cl_2Gm)_3(Bn\text{-}C_{16}H_{33})_2$[a]	$Co(Cl_2Gm)_3(Bn\text{-}C_{16}H_{33})_2$[a]			
parameter	240 K	40 K	LS[b]	295 K	HS[b]
metal ion	Fe^{2+}	Co^{2+}			
M–N1 (Å)	1.914(3)	1.908(5)	1.910	2.015(3)	2.062
M–N2 (Å)	1.904(3)	2.012(5)	1.970	1.970(3)	2.060
M–N3 (Å)	1.921(3)	2.031(5)	2.156	1.995(3)	2.072
B–O (Å)	av. 1.503	av. 1.528	av. 1.517	av. 1.515	av. 1.533
N–O (Å)	av. 1.362	av. 1.363	av. 1.338	av. 1.362	av. 1.338
C=N (Å)	av. 1.306	av. 1.312	av. 1.312	av. 1.283	av. 1.286
C–C (Å)	av. 1.434	av. 1.459	av. 1.465	av. 1.467	av. 1.493
B–C (Å)	1.568(5)	1.557(9)	1.584	1.542(5)	1.585
φ (deg)	17.5	3.1	17.6	1.9	0.3
α (deg)	39.3	39.2	41.1	39.1	39.6
h (Å)	2.38	2.51	2.51	2.51	2.56

[a]Only half of this molecule is symmetrically independent. [b]DFT-calculated values.

to its cobalt, nitrogen, and oxygen atoms. The total amount of calculated spin density for the HS state substantially exceeds that for the LS state. The nitrogen and oxygen atoms of the LS molecule of $Co(Cl_2Gm)_3(Bn\text{-}C_{16}H_{33})_2$ are not equally populated; the maxima of the spin density are localized on the atoms of its ribbed chelate fragment, giving the longest Co–N bond. This explains the observation of superhyperfine interaction with only two ^{14}N nuclei in the EPR spectrum of

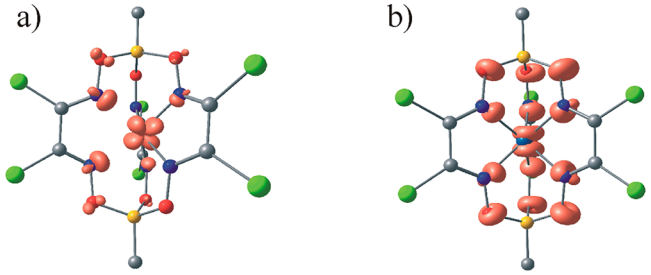

Figure 6. Spin-density distribution in the molecule $Co(Cl_2Gm)_3(Bn\text{-}C_{16}H_{33})_2$ for its doublet (a) and quartet (b) states.

the LS complex. In contrast, in the HS molecule of this cobalt(II) complex, the spin density is almost equally distributed close to its Co–N bonds and oxygen atoms of the donor oxime groups. The most prominent difference in the spin-density localization for such LS and HS states of $Co(Cl_2Gm)_3(Bn\text{-}C_{16}H_{33})_2$ is observed in the region of an encapsulated cobalt ion. The shape of such a density on this ion indicates d-orbital disposition, and the contribution of various orbitals into the spin population was analyzed using a natural bond orbital (NBO) scheme; the results obtained are summarized in Table 7. The main contribution in to its LS state is attributed to the $3d_{xy}$ orbital of an encapsulated cobalt ion: the orbital populations for most of the α and β 3d orbitals are almost equal, whereas those for α and β $3d_{xy}$ orbitals are 0.99 and 0.18 e. The substantial contribution of the $3d_{z^2}$ orbital is also observed: the populations of the corresponding α and β orbitals are 0.91 and 0.80 e, respectively. The contribution to the spin density in the HS molecule of $Co(Cl_2Gm)_3(Bn\text{-}C_{16}H_{33})_2$ is maximal in the cases of its $3d_{yz}$ and $3d_z^2$ orbitals, whereas the contribution of $3d_{xz}$ electrons of a caged cobalt ion is minimal.

DOI: 10.1021/acs.inorgchem.5b00546
Inorg. Chem. 2015, 54, 5827–5838

Table 7. Valence Orbital Populations (e) for the Molecule $Co(Cl_2Gm)_3(Bn\text{-}C_{16}H_{33})_2$ Deduced from NBO Analysis

	LS	HS
Co	7.76 [1.52 ($3d_{xy}$), 1.86 ($3d_{xz}$), 1.16 ($3d_{yz}$), 1.21 ($3d_{x^2-y^2}$), 1.71 ($3d_{z^2}$), 0.29 (4s)]	7.28 [1.38 ($3d_{xy}$), 1.76 ($3d_{xz}$), 1.22 ($3d_{yz}$), 1.38 ($3d_{x^2-y^2}$), 1.22 ($3d_{z^2}$), 0.32 (4s)]
N1	5.15 [1.32 (2s), 3.83 (2p)]	4.90 [1.57 (2s), 3.33 (2p)]
N2	5.17 [1.33 (2s), 3.84 (2p)]	4.44 [1.37 (2s), 3.07 (2p)]
N3	5.17 [1.35 (2s), 3.82 (2p)]	4.66 [1.50 (2s), 3.16 (2p)]
O1	5.84 [1.65 (2s), 4.85 (2p)]	5.84 [1.70 (2s), 4.14 (2p)]
O2	5.84 [1.65 (2s), 4.84 (2p)]	5.78 [1.56 (2s), 4.22 (2p)]
O3	5.84 [1.65 (2s), 4.83 (2p)]	5.83 [1.64 (2s), 4.19 (2p)]

The single-crystal X-ray data for the cobalt(II) hexachloroclathrochelate showed that a number of geometrical parameters of its CoN_6-coordination polyhedron suggest the presence of temperature SCO. In particular, this polyhedron at 40 K is characterized by the highest shift (Δ = 0.089 Å) of an encapsulated cobalt ion from the geometrical center of this polyhedron in the temperature range studied and the biggest φ value (3.1°) as well. These values decrease with the temperature up to 0.026−0.035 Å and 2.3°, respectively, while the Co−N3 distance that is the shortest at 40 K increases with the temperature (Table 1). An encapsulated cobalt ion has a significant anisotropy of its thermal ellipsoid at low temperature and is elongated in the direction perpendicular to the molecular C_2-symmetry axis (Figure 7). This fact seems to be a result of the superposition of two locations of such a caged cobalt ion, which is shifted in the direction of one of the two longest Co−N bonds, causing a decrease in the Δ and φ values.

Molecular Structures and Intermolecular Interactions. The apical long-chain alkyl substituents of the hexachloroclathrochelate $Fe(Cl_2Gm)_3(Bn\text{-}C_{16}H_{33})_2$ are ordered in the temperature range 168−300 K; the thermal ellipsoids of their carbon atoms undergo a thermal expansion only, and the ratio of the minimal and maximal principal mean-square atomic displacements almost remains (2.0−2.5). As a result, the crystal-to-crystal phase transition, experimentally detected using the DSC method for the fine-crystalline sample of $Fe(Cl_2Gm)_3(Bn\text{-}C_{16}H_{33})_2$ at T_{C-C1} = 173 K, was assigned to the movement of its apical hexadecyl substituents. We compared the geometries of FeN_6-coordination polyhedra and those of the long-chain alkyl substituents before and after this crystal-to-crystal phase transition (Figure 8a). In most cases, the average shift of their atoms (including hydrogen ones) from each other was rather small (<0.01 Å): the observed maximal shift for carbon and hydrogen atoms of the molecule $Fe(Cl_2Gm)_3(Bn\text{-}C_{16}H_{33})_2$ does not exceed 0.04 Å.

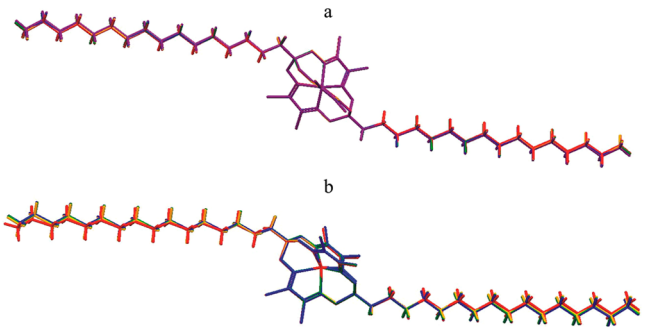

Figure 8. Molecular structures of $Fe(Cl_2Gm)_3(Bn\text{-}C_{16}H_{33})_2$ (a) at 168 K (red), 173 K (orange), 178 K (green), 183 K (blue), and 240 K (violet) and of $Co(Cl_2Gm)_3(Bn\text{-}C_{16}H_{33})_2$ (b) at 40 K (red), 230 K (orange), 240 K (green), and 260 K (blue).

The DSC curve upon cooling of the fine-crystalline sample of $Co(Cl_2Gm)_3(Bn\text{-}C_{16}H_{33})_2$ suggests two phase transitions in the temperature range 200−300 K (T_{C-C1} = 273 K and T_{C-C2} = 250 K) with the apical hexadecyl substituents disordered above 273 K. A comparison of the molecular structures of $Co(Cl_2Gm)_3(Bn\text{-}C_{16}H_{33})_2$ at various temperatures showed larger shifts of the carbon and hydrogen atoms of the long-chain alkyl substituents in the case of a cobalt(II) complex compared with its iron(II)-encapsulating analogue. For example, the average and maximal atomic shifts in the range 230−260 K exceed 0.2 and 0.4 Å, respectively, and reach as much as 0.13 and 0.25 Å for the clathrochelate $Co(Cl_2Gm)_3(Bn\text{-}C_{16}H_{33})_2$ at 40 K compared with those for higher temperatures (Figure 8b). After cooling, its single crystal was heated again; the temperature increase from 231 to 260 K was accompanied by lower atomic shifts in these apical substituents, and heating above 280 K was not accompanied by any disorder; this fact is also in good agreement with the DSC data.

Specific features of the intermolecular interactions in the crystals $Fe(Cl_2Gm)_3(Bn\text{-}C_{16}H_{33})_2$ and $Co(Cl_2Gm)_3(Bn\text{-}C_{16}H_{33})_2$ under these phase transitions were studied using the molecular Voronoi[23,24] and Hirshfeld surface[25,26] approaches. The molecular shapes obtained using such methods are similar (Figure 9): indeed, those are reported[35,36] to be complementary for the molecular crystals. Among 28 theoretically possible types of such interactions, both of these methods indicate an appearance of only eight types in the crystals under study (see Table S2 in the SI). Because an encapsulated metal ion and the capping boron atoms are almost completely isolated from the external factors,[34] the overwhelming majority of such interactions are the H···H contacts covering 65−70% of their molecular surfaces, while approximately 10% of these surfaces belong to the C−H···Cl interactions. At the same time,

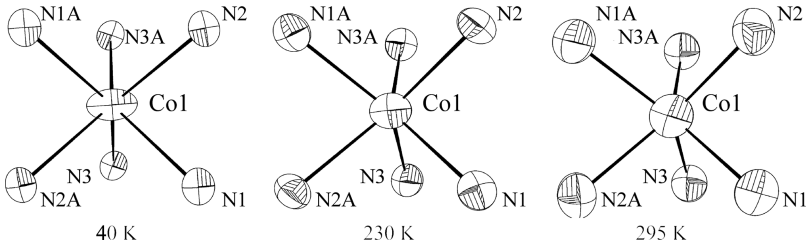

Figure 7. CoN_6-coordination polyhedra of an encapsulated cobalt(II) ion in the molecule $Co(Cl_2Gm)_3(Bn\text{-}C_{16}H_{33})_2$ at different temperatures. Thermal ellipsoids are given with p = 50%.

DOI: 10.1021/acs.inorgchem.5b00546
Inorg. Chem. 2015, 54, 5827−5838

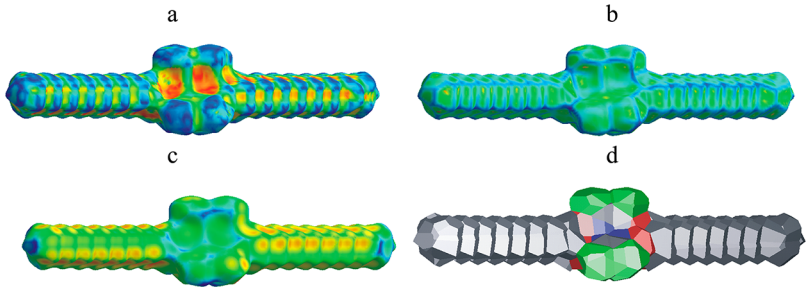

Figure 9. Hirshfeld surfaces for the molecule $Fe(Cl_2Gm)_3(Bn\text{-}C_{16}H_{33})_2$ at 168 K, which are mapped with a shape index (a), curvedness (b), and d_e (c), and that for the molecular Voronoi polyhedron (d).

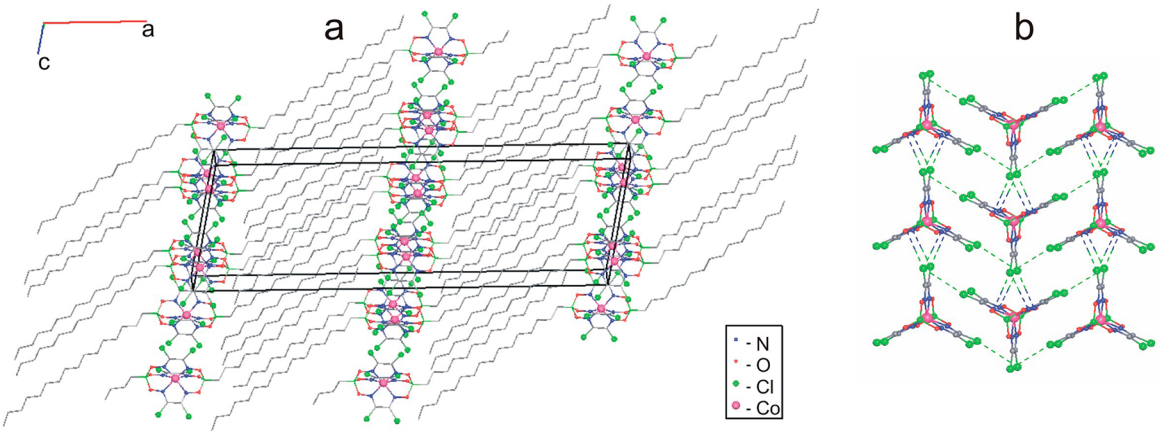

Figure 10. Crystal packing of the clathrochelate $Co(Cl_2Gm)_3(Bn\text{-}C_{16}H_{33})_2$: view along the crystal axis *b* (a) and the halogen bonding between its macrobicyclic molecules in the (011) plane (b). Hydrogen atoms are omitted for clarity.

the area of other intermolecular interactions (i.e., the H···O, Cl···Cl, Cl···O, Cl···N, Cl···C, and C···C supramolecular contacts) does not exceed 5% of the total surfaces. Both of these approaches do not reveal an appearance of any additional types of such interactions or abrupt change in their relative areas caused by the above structural phase transitions. The number of intermolecular contacts, estimated using the molecular Voronoi partitioning,[24] changes with the temperature and is different for these iron- and cobalt-containing crystals. At the same time, for both molecules $Fe(Cl_2Gm)_3(Bn\text{-}C_{16}H_{33})_2$ and $Co(Cl_2Gm)_3(Bn\text{-}C_{16}H_{33})_2$, the number of Cl···Cl, Cl···O, and Cl···N contacts remains unchanged, while the number of H···A (A = H, O, Cl) contacts depends on the temperature (see Table S1 in the SI), suggesting conformational stability of the cage frameworks and movement of their alkyl substituents. Indeed, these molecules form sandwiched layers packed parallel to the (011) plane (Figure 10a). Macrobicycles with a nonequivalent neighborhood of their chelate ribbed fragments are connected into the layers through Cl···Cl and π···Cl intermolecular interactions (Figure 10b) as short as 3.9 and 3.3 Å, respectively, and the interpenetrating long-chain alkyl substituents are situated between these layers.

The SCO behavior of the molecular compounds in the solid state can be regarded as a competition between long-range cooperative and short-range anticooperative interactions,[37] with stacking[38−40] and van der Waals bonding[7,41,42] typically regarded as anticooperative supramolecular interactions. So, gradual single-step SCO for the clathrochelate $Co(Cl_2Gm)_3(BThioph)_2$[14] can be assigned to the anticooperative effect of the π···S interactions in its crystals. In the isostructural crystals $Co(Cl_2Gm)_3(Bn\text{-}C_4H_9)_2$[13] and $Co(Br_2Gm)_3(Bn\text{-}C_4H_9)_2$,[15] the infinite π···Hal bonded chains with the shortest plane···dot distances of approximately 3.2−3.5 Å can be distinguished: the fine-crystalline samples of these *n*-butylboron-capped cobalt(II) hexahalogenoclathrochelates exhibit gradual SCO due to anticooperativity effects. The hexabromoclathrochelate $Co(Br_2Gm)_3(Bn\text{-}C_4H_9)_2$ also exhibits a "reverse" step on the $\mu_{eff}(T)$ curve that is absent for its hexachloroclathrochelate analogues. Thus, π···Hal supramolecular interactions substantially affect the SCO behavior of all of these cobalt(II) hexahalogenoclathrochelates; the "reverse" drop on the $\mu_{eff}(T)$ curve of the fine-crystalline samples of $Co(Br_2Gm)_3(Bn\text{-}C_4H_9)_2$ and $Co(Cl_2Gm)_3(Bn\text{-}C_{16}H_{33})_2$ is, probably, due to differences in the temperature behavior of the long- and short-range cooperativity effects in their crystals.

Visual analysis of the shape indexes and curvedness of d_e mapped on the Hirshfeld surfaces for the crystals $Fe(Cl_2Gm)_3(Bn\text{-}C_{16}H_{33})_2$ and $Co(Cl_2Gm)_3(Bn\text{-}C_{16}H_{33})_2$ at different temperatures revealed no significant changes under their crystal-to-crystal phase transitions (see Figures S2 and S3 in the SI). Taking into account that the majority of their molecular surfaces belong to the H···H interactions, such contributions were separated from other types of intermolecular interactions on 2D fingerprint plots shown in Figure 11 visualizing the changes under phase transitions. The phase transition in the crystal $Co(Cl_2Gm)_3(Bn\text{-}C_{16}H_{33})_2$ at 250 K caused changes in its 2D fingerprint plots for both short- and long-distance H···H contacts; only 2D plots at 225 and 235 K were found having points with 1.2 Å < $d_i \approx d_e$ < 1.3 Å (where d_i and d_e are the closest distances from the point to the nuclei interior and exterior to the molecular Hirshfeld surface), although in the former case, such points with d_i and d_e less than 1.4 Å appear

DOI: 10.1021/acs.inorgchem.5b00546
Inorg. Chem. 2015, 54, 5827−5838

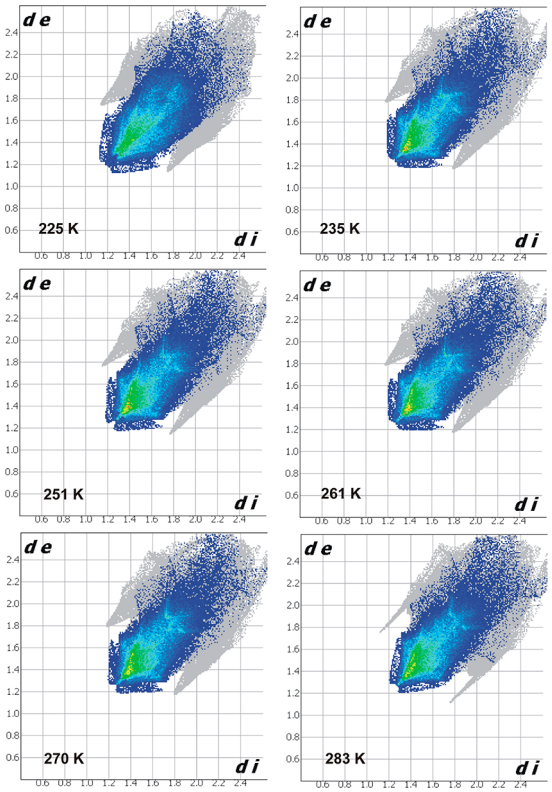

Figure 11. 2D fingerprint plots for the crystal $Co(Cl_2Gm)_3(Bn\text{-}C_{16}H_{33})_2$ at different temperatures resolved into H···H contacts. The full fingerprint appears beneath each decomposed plot as a gray shadow.

not very often (all of the points of a graph are shown in blue or green in Figure 11). Besides, such a plot at 225 K has a more diffuse character for the long-distance H···H interactions. The specific feature of a 2D plot at 283 K is the narrowed shape of its "wings" appearing as a result of formation of H···Cl contacts.

4. CONCLUSION

The synthesized *n*-hexadecylboron-capped iron and cobalt(II) hexachloroclathrochelates undergo temperature-induced SCO [for the paramagnetic cobalt(II) complex] and crystal-to-crystal phase transitions (for both of these clathrochelates) in the solid state. Analysis of the crystal packing reveals the conformational stability of the cage frameworks, with the structural rearrangements of the apical long-chain alkyl substituents being more pronounced for a macrobicyclic cobalt(II) complex; the observed unusual abrupt drop of its effective magnetic moment was assigned to such a structural transition. The fine-crystalline sample of this cobalt(II) hexachloroclathrochelate also undergoes anticooperative gradual and fully reversible spin transitions. The DFT-calculated parameters for its isolated molecule in the LS and HS states were found to be in excellent agreement with the experimental data, allowing localization of the spin density within a macrobicyclic framework. These experimental and theoretical data pave the way toward the successful synthesis of new "soft" magnetic materials.[43]

■ ASSOCIATED CONTENT

Ⓢ Supporting Information

CIF file, QS (mm s^{-1}) and *f* values for the iron(II) hexachloroclathrochelates, characteristics of the intermolecular interactions and the molecular Hirshfeld surfaces for the clathrochelates $Fe(Cl_2Gm)_3(Bn\text{-}C_{16}H_{33})_2$ and $Co(Cl_2Gm)_3(Bn\text{-}C_{16}H_{33})_2$ at different temperatures, and the coordinates of optimized structures. CCDC 1052216−1052219 and 1016991 for $Fe(Cl_2Gm)_3(Bn\text{-}C_{16}H_{33})_2$ and 1052220−1052229 and 1016989 for $Co(Cl_2Gm)_3(Bn\text{-}C_{16}H_{33})_2$ contain the supplementary crystallographic data for this paper. The Supporting Information is available free of charge on the ACS Publications website at DOI: 10.1021/acs.inorgchem.5b00546.

■ AUTHOR INFORMATION

Corresponding Authors

*E-mail: vologzhanina@mail.ru. Fax: +7-499-135-50-85.
*E-mail: voloshin@ineos.ac.ru. Fax: +7-499-135-50-85.

Notes

The authors declare no competing financial interest.

■ ACKNOWLEDGMENTS

The authors gratefully acknowledge support of the Russian Science Foundation (Project 14-13-00724). A.A.K. acknowledges the Council of the President of the Russian Federation (Grant MD-3589.2014.3) for financial support of the studies of the charge and spin density distributions. Y.Z.V. also thanks the Russian Academy of Sciences (Program 5) for support of the supramolecular studies.

■ DEDICATION

Dedicated to the 80th anniversary of Professor V. I. Minkin.

■ REFERENCES

(1) Halcrow, M. A. *Spin-Crossover Materials: Properties and Applications*; Wiley: New York, 2013.
(2) Kahn, O.; Martinez, C. J. *Science* **1998**, *279*, 44−48.
(3) Létard, J.-F.; Guionneau, P.; Goux-Capes, L. *Spin Crossover in Transition Metal Compounds III*; Topics in Current Chemistry; Springer: Berlin, 2004; pp 221−249.
(4) Meded, V.; Bagrets, A.; Fink, K.; Chandrasekar, R.; Ruben, M.; Evers, F.; Bernand-Mantel, A.; Seldenthuis, J. S.; Beukman, A.; van der Zant, H. S. J. *Phys. Rev. B* **2011**, *83*, 245415.
(5) Prins, F.; Monrabal-Capilla, M.; Osorio, E. A.; Coronado, E.; van der Zant, H. S. J. *Adv. Mater.* **2011**, *23*, 1545−1549.
(6) Hayami, S.; Moriyama, R.; Shigeyoshi, Y.; Kawajiri, R.; Mitani, T.; Akita, M.; Inoue, K.; Maeda, Y. *Inorg. Chem.* **2005**, *44*, 7295−7297.
(7) Hayami, S.; Shigeyoshi, Y.; Akita, M.; Inoue, K.; Kato, K.; Osaka, K.; Takata, M.; Kawajiri, R.; Mitani, T.; Maeda, Y. *Angew. Chem., Int. Ed.* **2005**, *44*, 4899−4903.
(8) Zhang, W.; Zhao, F.; Liu, T.; Yuan, M.; Wang, Z.-M.; Gao, S. *Inorg. Chem.* **2007**, *46*, 2541−2555.
(9) Hayami, S.; Kato, K.; Komatsu, Y.; Fuyuhiro, A.; Ohba, M. *Dalton Trans.* **2011**, *40*, 2167−2169.
(10) Vorontsov, I. I.; Potekhin, K. A.; Antipin, M. Y.; Voloshin, Y. Z.; Stash, A. I.; Belsky, V. K.; Dubovik, I. I.; Papkov, V. S. *Crystallogr. Rep.* **2001**, *46*, 758−770.
(11) Voloshin, Y. Z.; Lebedev, A. Y.; Novikov, V. V.; Dolganov, A. V.; Vologzhanina, A. V.; Lebed, E. G.; Pavlov, A. A.; Starikova, Z. A.; Buzin, M. I.; Bubnov, Y. N. *Inorg. Chim. Acta* **2013**, *399*, 67−78.
(12) Novikov, V. V.; Pavlov, A. A.; Belov, A. S.; Vologzhanina, A. V.; Savitsky, A.; Voloshin, Y. Z. *J. Phys. Chem. Lett.* **2014**, *5*, 3799−3803.
(13) Voloshin, Y. Z.; Varzatskii, O. A.; Novikov, V. V.; Strizhakova, N. G.; Vorontsov, I. I.; Vologzhanina, A. V.; Lyssenko, K. A.; Romanenko, G. V.; Fedin, M. V.; Ovcharenko, V. I.; Bubnov, Y. N. *Eur. J. Inorg. Chem.* **2010**, 5401−5415.

DOI: 10.1021/acs.inorgchem.5b00546
Inorg. Chem. 2015, 54, 5827−5838

(14) Belov, A. S.; Dolganov, A. V.; Novikov, V. V.; Vologzhanina, A. V.; Fedin, M. V.; Kuznetsov, E. V.; Bubnov, Y. N.; Voloshin, Y. Z. *Inorg. Chem. Commun.* **2013**, *29*, 160−164.
(15) Dolganov, A. V.; Belov, A. S.; Novikov, V. V.; Vologzhanina, A. V.; Romanenko, G. V.; Budnikova, Y. G.; Zelinskii, G. E.; Buzin, M. I.; Voloshin, Y. Z. *Dalton Trans.* **2015**, *44*, 2476−2487.
(16) Voloshin, Y. Z.; Dolganov, A. V.; Varzatskii, O. A.; Bubnov, Y. N. *Chem. Commun.* **2011**, *47*, 7737−7739.
(17) Voloshin, Y. Z.; Varzatskii, O. A.; Kron, T. E.; Belsky, V. K.; Zavodnik, V. E.; Strizhakova, N. G.; Palchik, A. V. *Inorg. Chem.* **2000**, *39*, 1907−1918.
(18) Ponzio, G.; Baldrocco, F. *Gazz. Chim. Ital.* **1930**, *60*, 415−420.
(19) Stoll, S.; Schweiger, A. *J. Magn. Reson.* **2006**, *178*, 42−55.
(20) Bain, G. A.; Berry, J. F. *J. Chem. Educ.* **2008**, *85*, 532.
(21) Sheldrick, G. M. *Acta Crystallogr., Sect. A* **2008**, *64*, 112−122.
(22) Dolomanov, O. V.; Bourhis, L. J.; Gildea, R. J.; Howard, J. a. K.; Puschmann, H. *J. Appl. Crystallogr.* **2009**, *42*, 339−341.
(23) Peresypkina, E. V.; Blatov, V. A. *Acta Crystallogr., Sect. B* **2000**, *56*, 1035−1045.
(24) Serezhkin, V. N.; Serezhkina, L. B.; Vologzhanina, A. V. *Acta Crystallogr., Sect. B* **2012**, *68*, 305−312.
(25) McKinnon, J. J.; Spackman, M. A.; Mitchell, A. S. *Acta Crystallogr., Sect. B* **2004**, *60*, 627−668.
(26) Spackman, M. A.; Jayatilaka, D. *CrystEngComm* **2009**, *11*, 19−32.
(27) Blatov, V. A.; Shevchenko, A. P.; Proserpio, D. M. *Cryst. Growth Des.* **2014**, *14*, 3576−3586.
(28) Wolff, S. K.; Grimwood, J. J.; McKinnon, J. J.; Turner, M. J.; Jayatilaka, D.; Spackman, M. A. *CrystalExplorer*, version 3.1; University of Western Australia: Crawley, Australia, 2012.
(29) Frisch, M. J.; Trucks, G. W.; Schlegel, H. B.; et al. *Gaussian 03*, revision E.01; Gaussian Inc.: Wallingford, CT, 2004.
(30) www.chemcraftprog.com.
(31) Voloshin, Y. Z.; Polshin, E. V.; Nazarenko, A. Y. *Hyperfine Interact.* **2002**, *141*−*142*, 309−320.
(32) Dolganov, A. V.; Belov, A. S.; Novikov, V. V.; Vologzhanina, A. V.; Mokhir, A.; Bubnov, Y. N.; Voloshin, Y. Z. *Dalton Trans.* **2013**, *42*, 4373−4376.
(33) Novikov, V. V.; Ananyev, I. V.; Pavlov, A. A.; Fedin, M. V.; Lyssenko, K. A.; Voloshin, Y. Z. *J. Phys. Chem. Lett.* **2014**, *5*, 496−500.
(34) Voloshin, Y. Z.; Kostromina, N. A.; Kramer, R. *Clathrochelates: Synthesis, Structure and Properties*; Elsevier: Amsterdam, The Netherlands, 2002.
(35) Prokaeva, M. A.; Baburin, I. A.; Serezhkin, V. N. *J. Struct. Chem.* **2009**, *50*, 867−872.
(36) Savchenkov, A. V.; Klepov, V. V.; Vologzhanina, A. V.; Serezhkina, L. B.; Pushkin, D. V.; Serezhkin, V. N. *CrystEngComm* **2015**, *17*, 740−746.
(37) Gütlich, P.; Garcia, Y.; Goodwin, H. A. *Chem. Soc. Rev.* **2000**, *29*, 419−427.
(38) Real, J. A.; Gallois, B.; Granier, T.; Suez-Panama, F.; Zarembowitch, J. *Inorg. Chem.* **1992**, *31*, 4972−4979.
(39) Létard, J.-F.; Guionneau, P.; Codjovi, E.; Lavastre, O.; Bravic, G.; Chasseau, D.; Kahn, O. *J. Am. Chem. Soc.* **1997**, *119*, 10861−10862.
(40) Boča, R.; Boča, M.; Dlháň, L.; Falk, K.; Fuess, H.; Haase, W.; Jaroščiak, R.; Papánková, B.; Renz, F.; Vrbová, M.; Werner, R. *Inorg. Chem.* **2001**, *40*, 3025−3033.
(41) Arata, S.; Torigoe, H.; Iihoshi, T.; Matsumoto, N.; Dahan, F.; Tuchagues, J.-P. *Inorg. Chem.* **2005**, *44*, 9288−9292.
(42) Halder, G. J.; Chapman, K. W.; Neville, S. M.; Moubaraki, B.; Murray, K. S.; Létard, J.-F.; Kepert, C. J. *J. Am. Chem. Soc.* **2008**, *130*, 17552−17562.
(43) Hayami, S.; Karim, M. R.; Lee, Y. H. *Eur. J. Inorg. Chem.* **2013**, 683−696.

DOI: 10.1021/acs.inorgchem.5b00546
Inorg. Chem. 2015, 54, 5827−5838